J. Ocean Univ. China (Oceanic and Coastal Sea Research)
DOI 10.1007/s11802-014-2331-0
ISSN 1672-5182, 2014 13 (6): 893-900
http://www.ouc.edu.cn/xbywb/
E-mail:xbywb@ouc.edu.cn

Wind Wave Characteristics and Engineering Environment of the South China Sea

WANG Zhifeng[1)], ZHOU Liangming[2), *], DONG Sheng[1)], WU Lunyu[3)], LI Zhanbin[4)], MOU Lin[4)], and WANG Aifang[5)]

1) *College of Engineering*, *Ocean University of China*, *Qingdao* 266100, *P. R. China*
2) *College of Physical and Environmental Oceanography*, *Ocean University of China*, *Qingdao* 266100, *P. R. China*
3) *The First Institute of Oceanography*, *State Oceanic Administration*, *Qingdao* 266061, *P. R. China*
4) *National Marine Data and Information Service*, *State Oceanic Administration*, *Tianjin* 300171, *P. R. China*
5) *Engineering Reconnaissance & Design Institute*, *Ocean University of China*, *Qingdao* 266100, *P. R. China*

(Received March 18, 2013; revised April 10, 2013; accepted August 25, 2014)

Abstract Wave simulation was conducted for the period 1976 to 2005 in the South China Sea (SCS) using the wave model, WAVEWATCH-III. Wave characteristics and engineering environment were studied in the region. The wind input data are from the objective reanalysis wind datasets, which assimilate meteorological data from several sources. Comparisons of significant wave heights between simulation and TOPEX/Poseidon altimeter and buoy data show a good agreement in general. By statistical analysis, the wave characteristics, such as significant wave heights, dominant wave directions, and their seasonal variations, were discussed. The largest significant wave heights are found in winter and the smallest in spring. The annual mean dominant wave direction is northeast (NE) along the southwest (SW)-NE axis, east northeast in the northwest (NW) part of SCS, and north northeast in the southeast (SE) part of SCS. The joint distributions of wave heights and wave periods (directions) were studied. The results show a single peak pattern for joint significant wave heights and periods, and a double peak pattern for joint significant wave heights and mean directions. Furthermore, the main wave extreme parameters and directional extreme values, particularly for the 100-year return period, were also investigated. The main extreme values of significant wave heights are larger in the northern part of SCS than in the southern part, with the maximum value occurring to the southeast of Hainan Island. The direction of large directional extreme H_s values is focus in E in the northern and middle sea areas of SCS, while the direction of those is focus in N in the southeast sea areas of SCS.

Key words surface waves; statistical characteristics; joint distributions; extreme parameters

1 Introduction

The South China Sea (SCS) is the largest semi-enclosed marginal sea in the northwest Pacific (Fig.1). It connects to the East China Sea (through Taiwan Strait), the Pacific Ocean (through Luzon Strait), the Sulu Sea, the Java Sea (through Gasper and Karimata Straits), and the Indian Ocean (through the Strait of Malacca). The study and prediction of wave conditions in SCS, such as wave characteristics and extreme parameters, have become more and more important in recent years because of the relevant increase in scientific and economic interests, such as wave power, marine engineering, and oil exploitation.

Qi *et al.* (1998) studied characteristics of ocean waves over the northern South China Sea from GEOSAT altimetry observations. Kohei *et al.* (1998) studied wave characteristics along the central coast of Vietnam in the South China Sea based on the measurements at a seaport from April 1997 to February 1998. Chu *et al.* (2004) studied wind-wave characteristics in SCS using TOPEX/ Poseidon data. However, all of the data used in those studies are affected by space and time limitations.

Numerical simulation method (hindcast and forecast) has become important for wave studies since the appearance of numerical models. Wang *et al.* (1992) applied the Wave Model (WAM) to the wave hindcast under conditions of two typhoons and two cold fronts near Hong Kong in the northern part of the South China Sea. Qiao *et al.* (1997) simulated wave fields under tropical cyclones in the Gulf of Tonkin and estimated wave environmental and extreme parameters. Zhu *et al.* (2003) established a coupled mathematical model of nearshore waves, tide and current under tropical cyclones in the SCS. Zhou *et al.* (2008) simulated the sea wave directional spectra under typhoon wind forcing in the SCS using WAVEWATCH-III. Chu and Cheng (2008) investigated wave characteristics in the SCS during the passage of Typhoon Muifa in 2004 winter. Zheng *et al.* (2011, 2012) estimated wind energy

* Corresponding author. Tel: 0086-532-66781511
E-mail: zhou5299@ouc.edu.cn

and wave energy resources in the SCS. Zhou *et al.* (2008) studied the effect of surface waves on air-sea momentum flux under high wind conditions during typhoons in the SCS. Zhang *et al.* (2009) studied wind wave effects on ocean circulation in the SCS.

More comprehensive and detailed wave information is needed in environmental research and engineering design. This study aim to improve the understanding of waves in the SCS and provide basic information for promoting environmental research and beuefiing engineering design.

In Section 2, the progress in the numerical wave simulation is described, including the wind input and the wave output. In Section 3, the wave characteristics and engineering environment, such as seasonal variations, joint distributions and wave extreme values, are investigated. The summary and conclusions are given in Section 4.

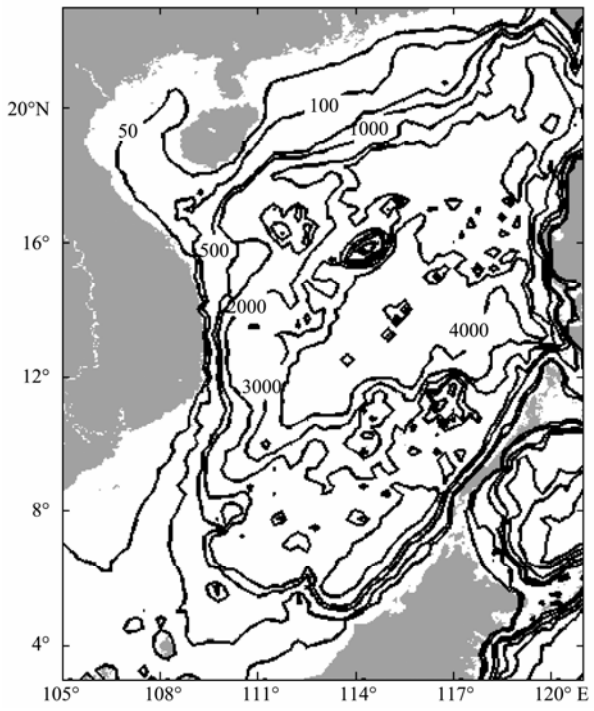

Fig.1 Depth contours of South China Sea (m).

2 Numerical Simulations

2.1 Wind Input

The forcing for the wave modeling is the re-analysis winds. The wind model, the Weather Research and Forecasting (WRF), is used to simulate tropical storms (Gu *et al.*, 2005; Yang *et al.*, 2008). The simulation assimilated station-observed data, QuickSCAT data, and data from weather chart and typhoon (or tropical cyclone) yearbooks. The simulation period is from 1976 to 2005, with a horizontal resolution of 0.2˚ and a time interval of 3 h.

Comparisons were carried out between the assimilated winds and observations at Dongsha station (20˚40′N, 116˚43′E), Xisha station (16˚50′N, 112˚20′E) and Nansha station (9˚23′N, 112˚53′E) (Fig.2). The time span is from 2000 to 2005. The mean errors of wind speeds at the three stations are 2.7, 3.4 and 1.9 m s^{-1}, and these of wind directions are 25˚, 26˚ and 29˚, respectively.

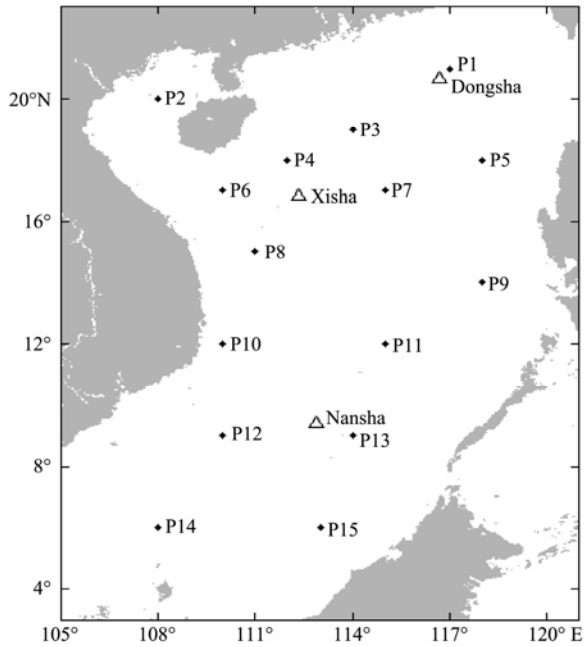

Fig.2 Wind observation stations and selected points for wave statistical analysis.

The TOPEX/Poseidon data were also used to verify the accuracy of wind fields. Here, the comparisons of wind speeds between the assimilation and altimetry observations are shown in Fig.3. The two tracks correspond to the periods from 21 to 31 October 2004 and from 10 to 20 November 2004, respectively. The results show that the wind fields produced from the reanalysis method well agree with the TOPEX/Poseidon data. Four tropical cyclones were chosen as examples to calibrate the assimilated wind under high wind conditions. Fig.4 shows the comparisons of the maximum wind speeds at the center of Typhoon Sam from 20 to 23 August, 1999 and Typhoon Wukong from 6 to 10 September, 2000. It can be seen that the calculated and observed wind speeds show a good consistency.

2.2 Wave Simulations

The wave model WAVEWATCH III (WW III) (Tolman, 2009) is applied in this paper. The model was developed by the National Oceanic and Atmospheric Administration-National Centers for Environmental Prediction (NOAA-NCEP). It is designed with the general governing transport equations that permit full coupling with ocean models, improved physics integration schemes, improved propagation schemes (third order), and improved physics of wave growth and decay. The WW III has been used in many research programs to study surface wave dynamics. As the operational wave model of the NCEP for global and regional wave forecast it was validated over a global-scale wave forecast and a regional wave forecast (Hara and Belcher, 2002; Moon *et al.*, 2004).

The WW III grid in this study extends from 3.0˚ to 25.0˚N, 99.0˚ to 125.0˚E, with a horizontal resolution of

0.2˚ by 0.2˚. The output time period is from 1 January 1976 to 31 December 2005 with an hourly time interval.

Comparisons were conducted between the model hindcast results and the TOPEX/Poseidon altimeter observations. Synchronous with wind speeds, comparisons of significant wave heights H_s are shown in Fig.5. The time series cover the same periods from 21 to 31 October, 2004 and from 10 to 20 November, 2004 as TOPEX/Poseidon passed over the SCS. The simulation results are consistent with the observations, which indicates that in general the WW III can well reproduce the surface wave field in the SCS.

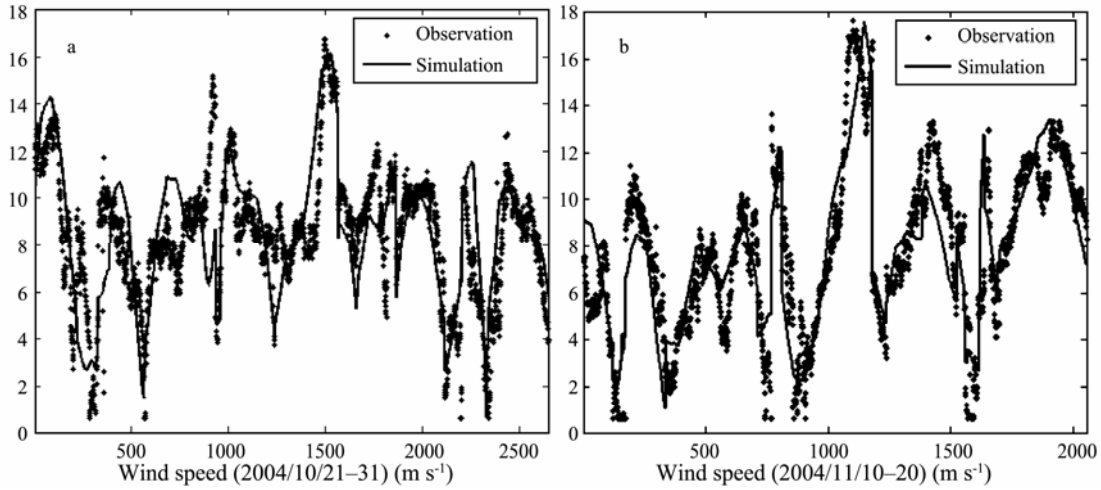

Fig.3 Comparisons of wind speed between the simulation and T/P altimeter observations.

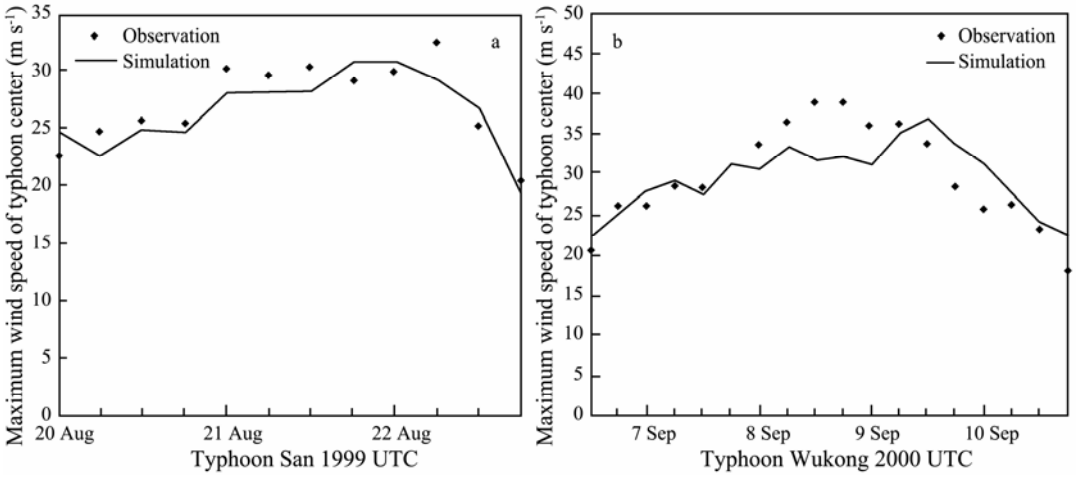

Fig.4 Comparisons of the maximum wind speed between the simulation and typhoon yearbooks at the center of (a) Typhoon Sam and (b) Typhoon Wukong.

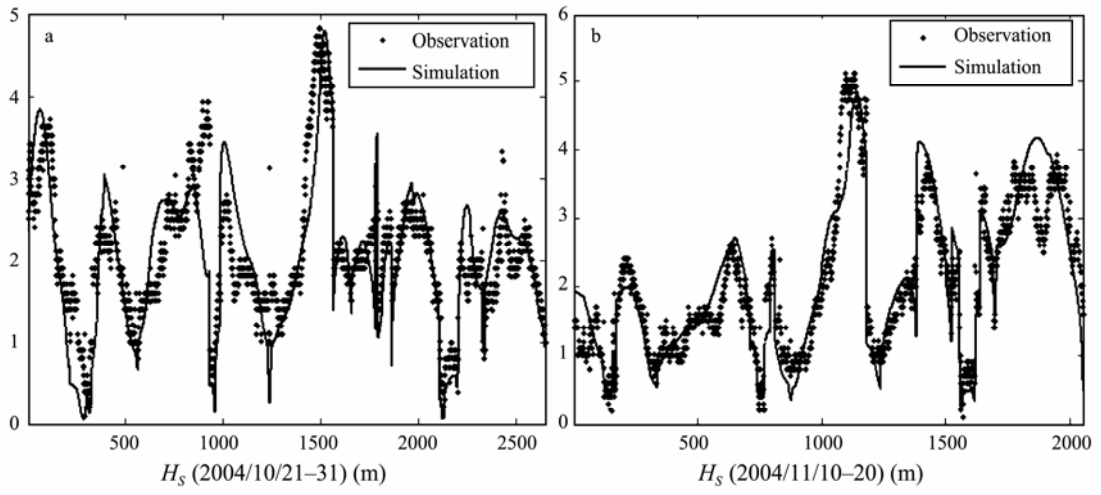

Fig.5 Comparisons of H_s (m) between the simulation and T/P altimeter observations.

Observed wave data under typhoon winds are scarce. Three datasets are available during the passages of Typhoon Wayne (1986), Typhoon Brian (1989) and Typhoon Damrey (2005). The comparisons of H_s between the measurements and model simulations during the typhoon passages are listed in Table 1. The simulated results are very close to the observed values, indicating that the WW III can be a dependable model to simulate surface waves under typhoon conditions in the SCS.

Table 1 Comparisons of H_s between the simulation and observations during the passages of typhoons.

Typhoon	Observation time	Longitude (E)	Latitude (N)	Observation (m)	Simulation (m)
Wayne	06:00 September 5, 1986	112˚07.6′	19˚32.8′	8.6	8.9
Brian	12:00 September 30, 1989	112˚07.6′	19˚32.8′	8.7	9.0
Damrey	03:00 September 26, 2005	109˚07.4′	19˚46.8′	7.2	7.4

3 Statistical Analysis and Engineering Environment

In order to illustrate the wave characteristics in the SCS, fifteen points were selected, which are located in the northern, central and southern parts of the study area (Fig.2 and Table 2).

3.1 Seasonal Variations of Wave Heights and Directions

The SCS is under the influence of monsoon winds and synoptic systems such as fronts and tropical cyclones (Wang *et al.*, 2009; Wang *et al.*, 2007). In general, the winter monsoon season is from October to March, during which northeast wind prevails and cold fronts influence the SCS; the summer monsoon season is from June to August, with anticyclones and enhanced convection migrating northward from the equator to the mid-latitudes. The sea-surface wind over the SCS is strongest during the winter monsoon and weaker during the summer monsoon. In the periods of seasonal transition, spring and autumn, the average wind speed is smaller than in summer and winter. The tropical cyclone (TC) is a very important weather factor that influences the SCS in summer and autumn. The central and northern parts of the SCS (19˚–20˚N, 110˚–120˚E) is the most important region where the TC forms. In the SCS, the propagating direction of the TC is mainly west-forward and more than 25 TCs occur every year, mostly from July to October.

Fig.6 shows the seasonal variations of H_s and dominant

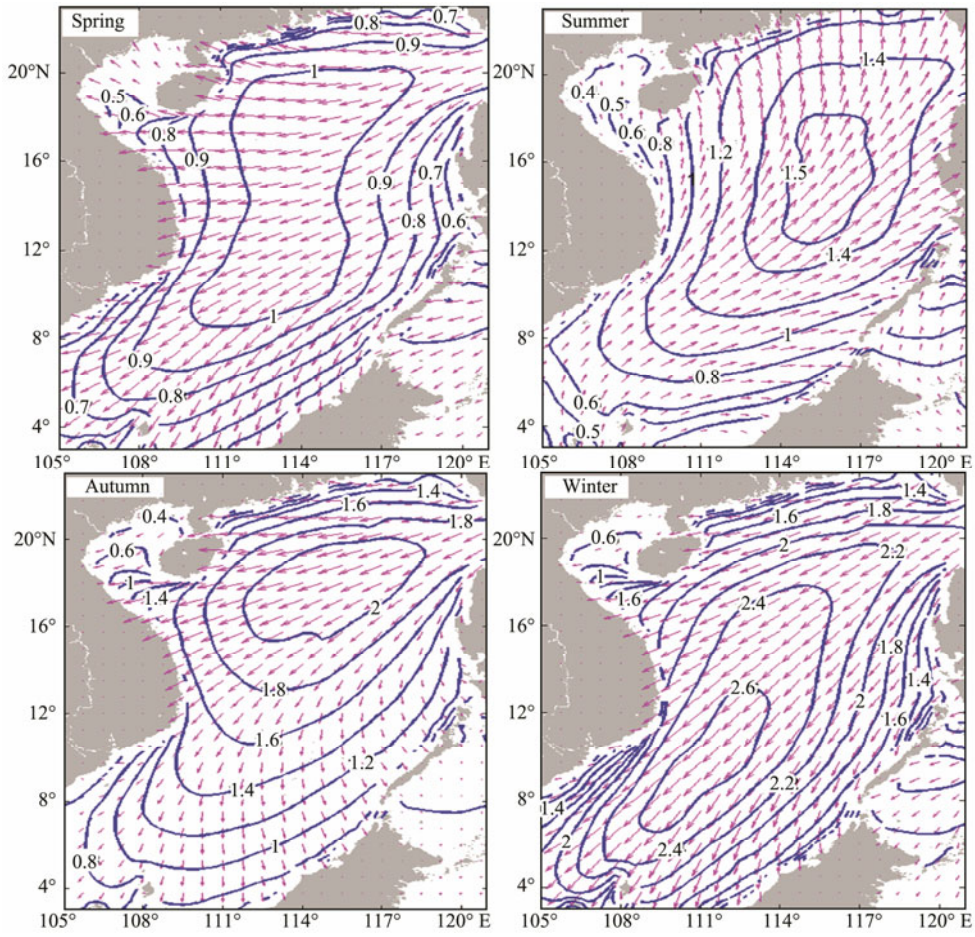

Fig.6 Seasonal distributions of H_s (m) and D_{ir}.

wave direction D_{ir} in the SCS. During spring, D_{ir} is southwestward along the diagonal line across the SCS from southwest to northeast, south southwestward in the southeast SCS, and westward in most of the northwest SCS with northwestward waves in the Beibu Bay. During summer, D_{ir} becomes northeastward along the southwest to northeast diagonal line, north northeastward in the northwest SCS, and eastward in the southeast SCS. During autumn, D_{ir} is again southwestward along the southwest to northeast diagonal line and in the northwest SCS, and south southwestward in the southeast SCS. Influenced by strong winter monsoon, D_{ir} is southwestward in most of the SCS during winter. By comparing the seasonal significant wave heights, it can be seen that the maximum value of H_s is largest in winter and smallest in spring. In spring, H_s in the central SCS (10° to 20°N, 111° to 115°E) is greater than 1m with the maximum value greater than 1.5 m; outside the area H_s is smaller than 1m. The maximum H_s greater than 2 m occurs in the northern SCS during autumn, whereas the maximum H_s can reach up to 2.6 m in the southwestern SCS in winter.

Fig.7 shows the annual spatial distributions of H_s and D_{ir} in the SCS. Generally, D_{ir} is southwestward along the diagonal line across the SCS from southwest to northeast, west southwestward in the northwest SCS, and south southwestward in the southeast SCS. The maximum H_s is greater than 1.7 m, occurring in the central SCS. The isolines are ellipsoidal, with the long axes in southwest to northeast direction.

3.2 Joint Distributions

Joint distributions of wave heights and wave periods (directions) were applied in this study for the analysis of wave fields (Dag and Fouques, 2010; Soares and Carvalho, 2012). Fig.8 is the joint distributions of H_s and T_s at 10 points. A common feature shown in the figure is a single peak at each location, which corresponds to a wave period around 4.5 s. With a frequency greater than 1%, H_s is smaller than 5 m, while T_s ranges from 2 to 10 s.

The joint distributions of H_s and D_{ir} show a double-peak pattern (Fig.9). The significant wave height corresponding to the peak frequencies range from 0.5 to 1.5 m. The distribution characteristics of D_{ir} are consistent with the analysis in the previous section. The dominant D_{ir} are westward or southwestward in most of the SCS, while the secondary D_{ir} is northward or northwestward.

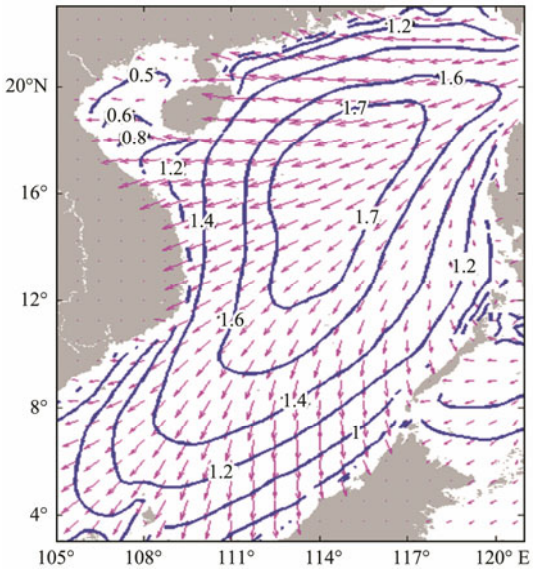

Fig.7 Annual distributions of H_s (m) and D_{ir}.

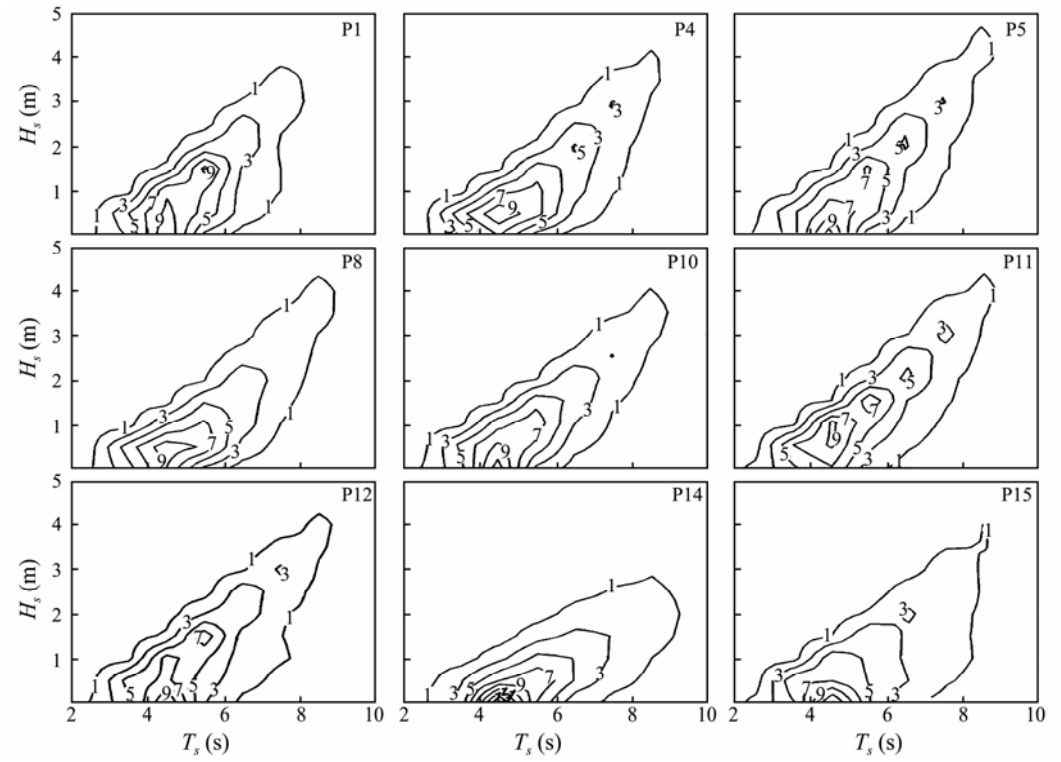

Fig. 8 Joint distributions of H_s (m) and T_s (s).

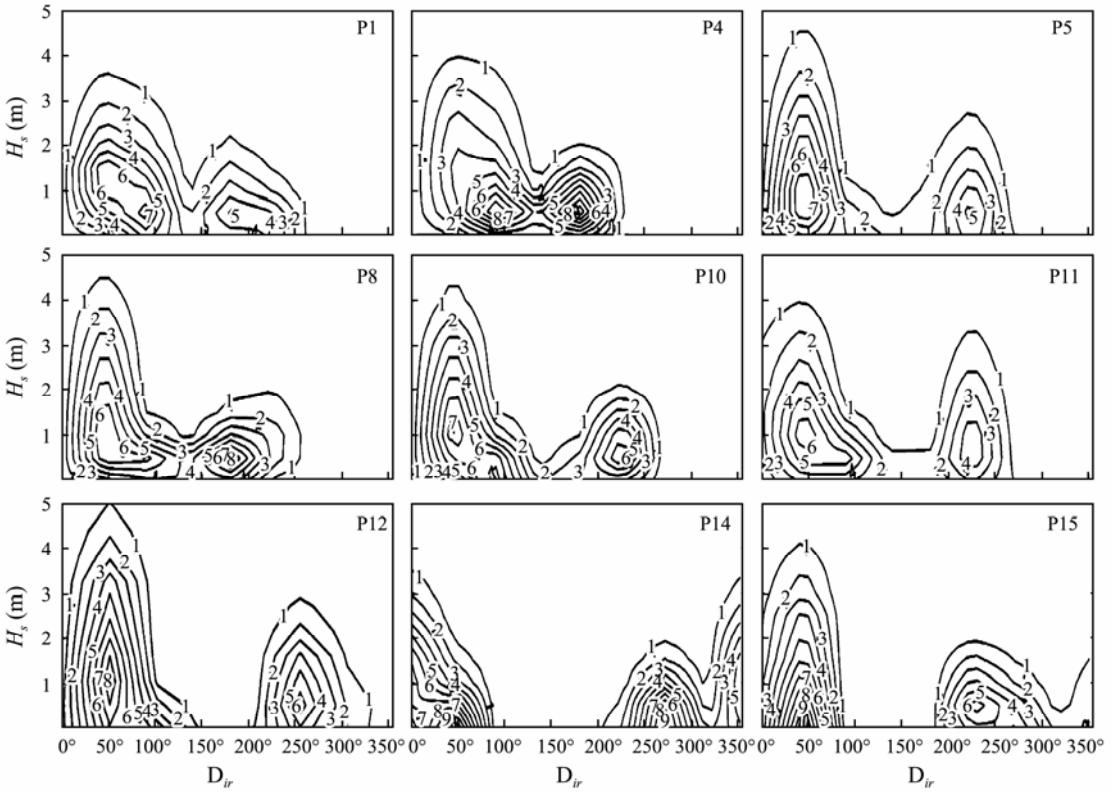

Fig.9 Joint distributions of H_s (m) and D_{ir}.

3.3 Wave Extreme Parameters

In order to obtain reliable extrapolation for wave extreme parameters, three well-known extreme value distributions, the Pearson III distribution, Gumbel distribution and Weibull distribution were compared. The Weibull distribution is found to be suitable for the long-term inference of extreme values in the SCS.

Extreme values of H_s and T_s, were calculated for different return periods. Fig.10 shows the spatial distributions of H_s and T_s for 100-year return period in the SCS. It can be seen that the maximum value of H_s, greater than 18 m, occurs to the southeast of Hainan Island. The extreme values of H_s are larger in the northern SCS than those in the southern. In the central SCS, the values are greater than 12 m. The extreme values of H_s decrease to 6 m in the southwest corner of the SCS and in the northern Tonkin Gulf, and reach up to 11 m at the mouth of the Gulf. Those results are consistent with those of Kohei *et al.* (1998). As shown in Fig.10, the larger T_s values,

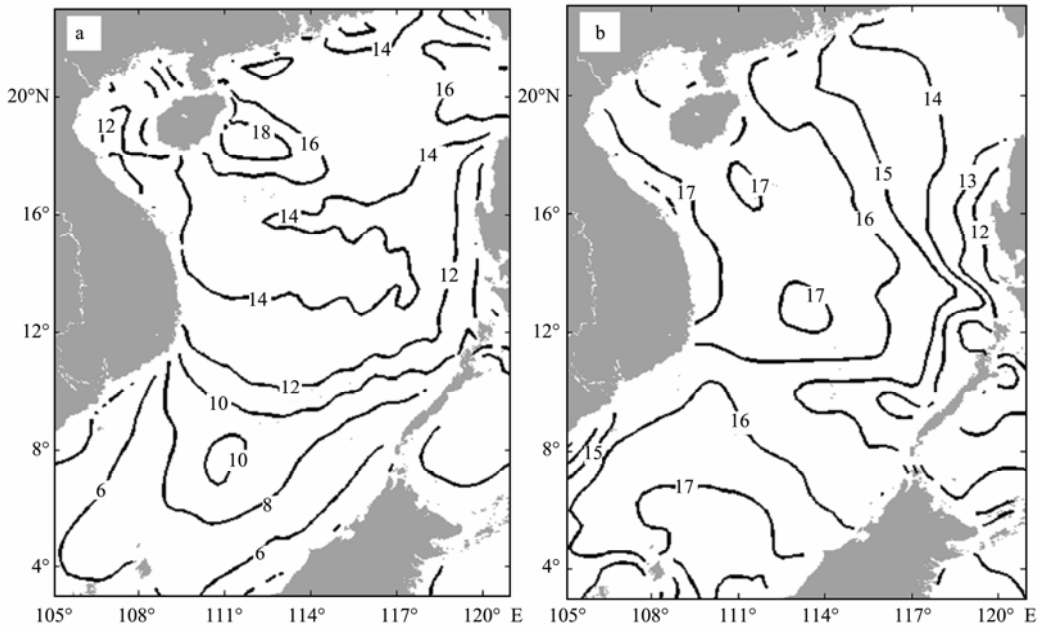

Fig.10 The spatial distributions of a) H_s (m) and b) T_s (s) for 100-year return period.

with the maximum value greater than 17 s, occur in the western SCS, while the smaller values, with the minimum value less than 12 s occur in the eastern SCS. In most of the SCS the T_s values are larger than 12 s. The larger values are also found in the southern SCS, with the maximum greater than 17 s.

The directional extreme H_s values at 15 points are listed in Table 2. The waves with the maximum heights are found propagating in the westward direction in most of the northern and central SCS. The secondary extreme values are mainly in the southwest and occasionally in the northwest direction. In the southeast SCS, the waves with the maximum heights are propagating in the south southwest direction.

Table 2 H_s (m) for 100-year return period in 8 directions

	Longitude (E)	Latitude (N)	N	NE	E	SE	S	SW	W	NW
P1	117°	21°	7.17	12.48	14.34	12.05	11.76	10.75	8.60	7.03
P2	108°	20°	6.94	11.34	11.57	8.21	8.33	4.86	5.21	6.02
P3	114°	19°	9.00	13.28	14.76	14.61	11.07	10.92	9.00	9.45
P4	112°	18°	8.02	16.05	18.66	15.30	9.70	8.21	8.58	9.14
P5	118°	18°	10.84	13.48	13.90	12.09	10.29	10.84	9.59	8.90
P6	110°	17°	12.47	14.39	14.84	13.06	11.72	6.83	6.08	8.31
P7	115°	17°	9.95	13.41	14.47	15.07	8.14	9.49	8.89	9.04
P8	111°	15°	8.10	13.85	14.73	9.87	7.81	6.04	7.07	6.19
P9	118°	14°	9.63	11.13	13.57	10.58	5.84	9.77	11.40	9.09
P10	110°	12°	7.54	13.22	11.50	3.97	4.23	4.23	5.02	5.68
P11	115°	12°	10.82	13.36	11.09	6.95	9.62	8.55	6.28	10.69
P12	110°	9°	6.21	8.74	6.38	1.66	2.19	5.51	4.81	5.59
P13	114°	9°	9.23	5.91	6.46	6.46	5.81	6.28	6.46	5.54
P14	108°	6°	5.08	7.47	2.24	2.32	3.29	3.44	2.99	2.02
P15	113°	6°	7.11	3.98	1.07	1.99	2.99	6.54	6.61	5.55

4 Summary

In this paper, wave fields are simulated by WAVEWATCH-III from 1976 to 2005. The wind input data is from the objective reanalysis wind datasets. Comparisons of wave heights between the simulation and observations show a good agreement.

From the statistical analysis, several wave characteristics can be summarized as follows: 1) the annual mean dominant wave direction is southwestward along the diagonal line across the SCE from southwest to northeast, west southwestward in the northwest SCS, and south southwestward in the southeast SCS; 2) the significant wave height is largest in winter and smallest in spring; 3) the joint distribution results show a single-peak pattern for H_s and T_s, but a double-peak for H_s and D_{ir}; 4) the extreme values of H_s are larger in the northern SCS than in the southern SCS, and the maximum value appears to the southeast of Hainan Island; 5) the direction of large directional extreme H_s values is focus in E in the northern and middle sea areas of SCS, while the direction of those is focus in N in the southeast sea areas of SCS.

Acknowledgements

This work is supported by the National Natural Science Foundation of China (51279186) and the Open Fund of the Shandong Province Key Laboratory of Ocean Engineering, Ocean University of China (201362045).

References

Chu, P. C., and Cheng, K. F., 2008. South China Sea wave characteristics during Typhoon Muifa passage in winter 2004. *Journal of Oceanography*, **64** (1): 1-21.

Chu, P. C., Qi, Y. Q., Chen, Y. C., Shi, P., and Mao, Q. W., 2004. South China Sea wind-wave characteristics. Part 1: Validation of Wavewatch-III using TOPEX/Poseidon data. *Journal of Atmospheric and Oceanic Technology*, **21** (11): 1718-1733.

Dag, M., and Fouques, S., 2010. A joint distribution of significant wave height and characteristic surf parameter. *Coastal Engineering*, **57** (10): 948-952.

Gu, J. F., Xiao, Q. N., Kuo, Y. H., Barker, D. M., Xue, J. S., and Ma, X. X., 2005. Assimilation and simulation of Typhoon Rusa (2002) using the WRF system. *Advances in Atmospheric Sciences*, **22**: 415-427.

Guedes, S. C., and Carvalho, A. N., 2012. Probability distributions of wave heights and periods in combined sea-states measured off the Spanish. *Ocean Engineering*, **52**: 13-21.

Hara, T., and Belcher, S. E., 2002. Wind forcing in the equilibrium range of wind-wave spectra. *Journal of Fluid Mechanics*, **470**: 223-245.

Kohei, N., Shinji, K., and Dao, X. Q., 1998. Wave characteristics on the central coast of Vietnam in the South China Sea. *Coastal Engineering Journal*, **40** (4): 347-366.

Moon, I. J., Ginis, I., and Hara, T., 2004. Effect of surface waves on air-sea momentum exchange. Part II: Behavior of drag coefficient under tropical cyclones. *Journal of the Atmospheric Sciences*, **61**: 2334-2348.

Qi, Y. Q., Shi, P., and Mao, Q. W., 1998. Characteristics of sea wave over the northern South China Sea from GEOSAT altimetric observations. *Acta Oceanologica Sinica*, **20** (2): 20-26 (in Chinese).

Qiao, F. L., Yu, W. D., and Pan, Z. D., 1997. Study on the wind and wave extreme parameters of Tonkin Gulf in the South China Sea–the applications of LAGFD numerical models. *Journal of Hydrodynamics*, **12** (1): 75-86 (in Chinese).

Tolman, H. L., 2009. *User Manual and System Documentation of WAVEWATCH-III Version 3.14*. NOAA/NWS/NCEP/MMAB Technical Note, Washington, 1-194.

Wang, B., Huang, F., Wu, Z. W., Yang, J., Fu, X., and Kikuchi, K., 2009. Multi-scale climate variability of the South China Sea monsoon: A review. *Dynamics of Atmospheres and Oceans*, **47**: 15-37.

Wang, G. H., Su, J. L., Ding, Y. H., and Chen, D. K., 2007. Tropical cyclone genesis over the South China Sea. *Journal of Marine Systems*, **68**: 318-326.

Wang, W. Z., Chen, J. C., and Li, M. Q., 1992. Wind waves simulation in the North Area of the South China Sea. *Chinese Journal of Oceanology and Limnology*, **10** (2): 107-118.

Yang, S. H., Kang, K. R., Cui, X. P., and Wang, H. J., 2008. Diagnostic analysis of the asymmetric structure of the simulated landfalling typhoon 'Haitang'. *Progress in Natural Science*, **18** (10): 1249-1260.

Zhang, H., Sannasiraj, S. A., and Chan, E. S., 2009. Wind wave effects on hydrodynamic modeling of ocean circulation in the South China Sea. *The Open Civil Engineering Journal*, **3**: 48-61.

Zheng, C. W., Zheng, Y. Y., and Chen, H. C., 2011. Research on wave energy resources in the northern South China Sea during recent 10 years using SWAN wave model. *Journal of Subtropical Resources and Environment*, **6** (2): 54-59 (in Chinese).

Zheng, C. W., Zhuang, H., Li, X., and Li, X. Q., 2012. Wind energy and wave energy resources assessment in the East China Sea and South China Sea. *Science China Technological Sciences*. **55** (1): 163-173.

Zhou, L. M., Wang, A. F., and Guo, P. F., 2008. Numerical Simulation of sea surface directional wave spectra under typhoon wind forcing. *Journal of Hydrodynamics*, **20** (6): 776-783.

Zhou, L. M., Wang, A. F., Guo, P. F., and Wang, Z. F., 2008. Effect of surface waves on air-sea momentum flux in high wind conditions for typhoons in the South China Sea. *Progress in Natural Science*, **18** (9): 1107-1113.

Zhu, L. S., Song, Y. F., Qiu, Z., Chen, X. H., Mai, B. Q., Qiu, Y. W., and Song, L. L., 2003. Computation of wave, tide and wind currents for the South China Sea under tropical cyclones. *China Ocean Engineering*, **17** (4): 505-516.

(Edited by Xie Jun)